SCT Barrel Module FDR Document

SCT Barrel Module : Mechanical and Thermal Performance

Abstract

This document describes module metrology results and the measurements of a thermal module.

Prepared by :	*Checked by :*	*Approved by :*
R. Apsimon, A Carter, J. Carter, Y. Unno		

Distribution List

Table of Contents

1 SCOPE OF THE DOCUMENT

Metrology results are presented for barrel modules in section 2 and thermal results in section 3. The measured thermal properties of modules are compared with FEA calculation. Over a period of several years during the evolution of the module design, special *thermal modules* have been built for detailed thermal study, and in particular to check the FEA calculations regarding thermal runaway of irradiated detectors. Agreement has been good. A new thermal module has recently been constructed and first results are presented in section 3.

2 BARREL MODULE METROLOGY RESULTS

2.1 Metrology of completed modules

Assembled modules have been surveyed for their mechanical precision, both in-plane and out-of-plane, as defined in SCT-BM-FDR-7. The measurements were made with a 3D metrology machine. One such machine used is shown in Figure 1. This machine has an absolute precision of better than 1 μm in the (x y) - plane over a span of 100 mm x 100 mm, and better than 10 μm in the z direction with auto-focusing.

Figure 1 A 3D metrology machine, Mitutoyo QuickVision Pro250

2.2 In-Plane Survey

The reduced parameter set is defined for the in-plane survey in SCT-BM-FDR-7, section 3.2.1. The parameter and tolerance list is reproduced in Table 1. The survey results, giving deviations from the design values, are shown in Figures 2 to 4 for a sample of seven modules constructed by the Japanese cluster. Figure 2 shows the positions of the dowel hole and slot, Figure 3 the centre and separation of the pairs of sensors, and Figure 4 the rotation of the sensors and the half-stereo angle. In each figure, the tolerance on the quantity is half the span of the horizontal axis. Similar results are obtained for modules made by the UK-B cluster[1]

Parameter	Design Value	Tolerance
Dowel hole, mhx [µm]	-6500	30
Dowel hole, mhy [µm]	-37500	30
Dowel slot, msx [µm]	38500	100
Dowel slot, msy [µm]	-37500	30
Mid-point of front pair, midxf [µm]	0	10
Mid-point of front pair, midyf [µm]	0	5
Separation of front pair, sepf [µm]	64090	10
Separation of back pair, sepb [µm]	64090	10
Sensor1 angle, a1 [mrad]	0	0.13
Sensor2 angle, a2 [mrad]	0	0.13
Sensor3 angle, a3 [mrad]	0	0.13
Sensor4 angle, a4 [mrad]	0	0.13
Half stereo angle, half-stereo [mrad]	-20	0.13

Table 1: Module in-plane geometry parameters

For all the parameters, the main parts of the distributions are well within the tolerances. However, occasionally, there is a measurement at the limit of the tolerance. Also, there are slight offsets in the centres of the distributions of the sensor angles. From these measurements we conclude:

(1) The present assembly jigs and assembly processes conform to the requirements

(2) Although the jigs are engineered to the limit, some fine tuning may still be possible

(3) Good control can be maintained during series production through the measurement and monitoring of these distributions, feeding the results back into the module assembly process.

[1] http://www.slac.stanford.edu/~stevemc/metrology.pdf

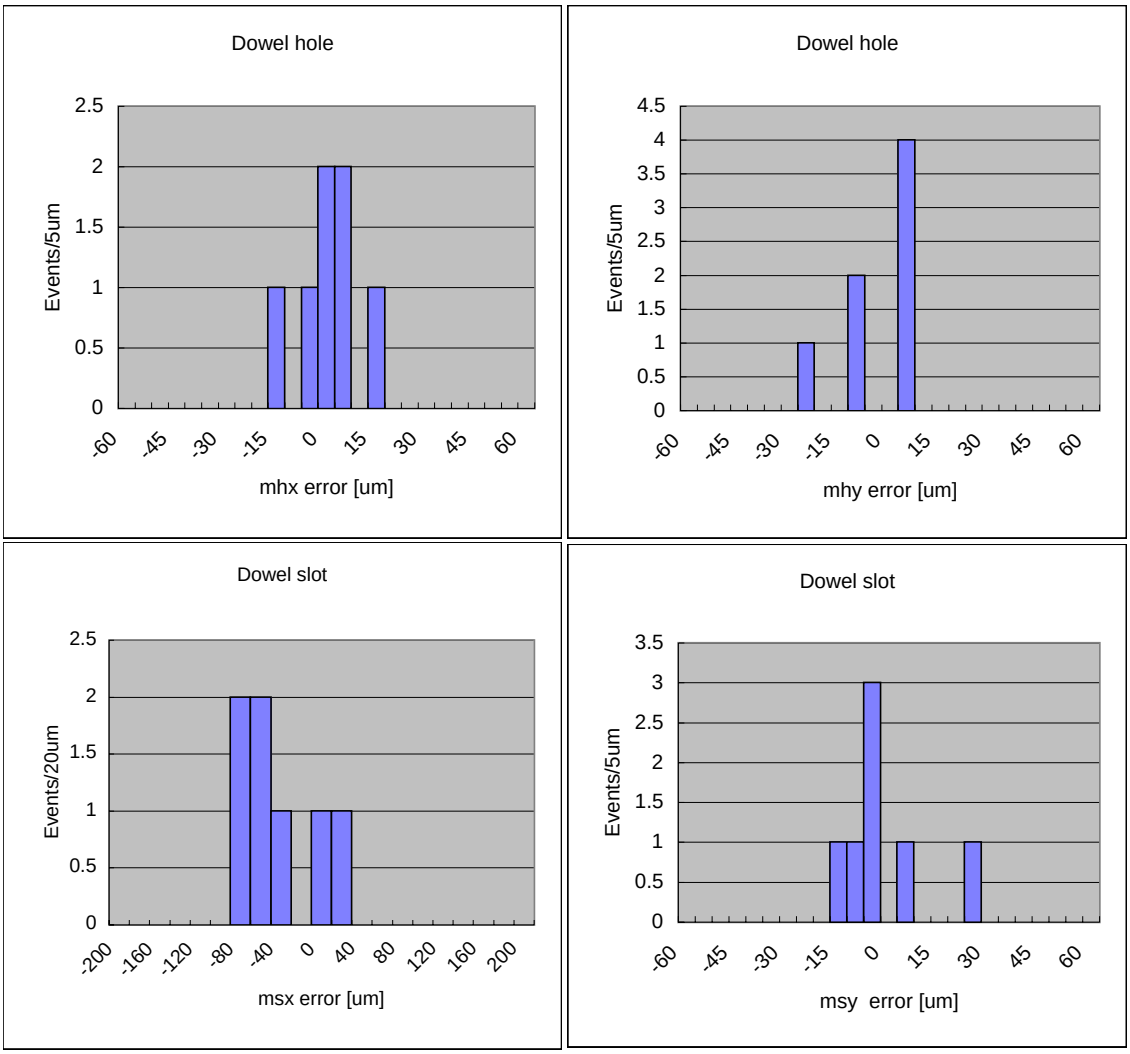

Figure 2 In-plane survey: deviations from the nominal of mhx and mhy of the dowel hole and msx and msy of the slot in the BeO facing

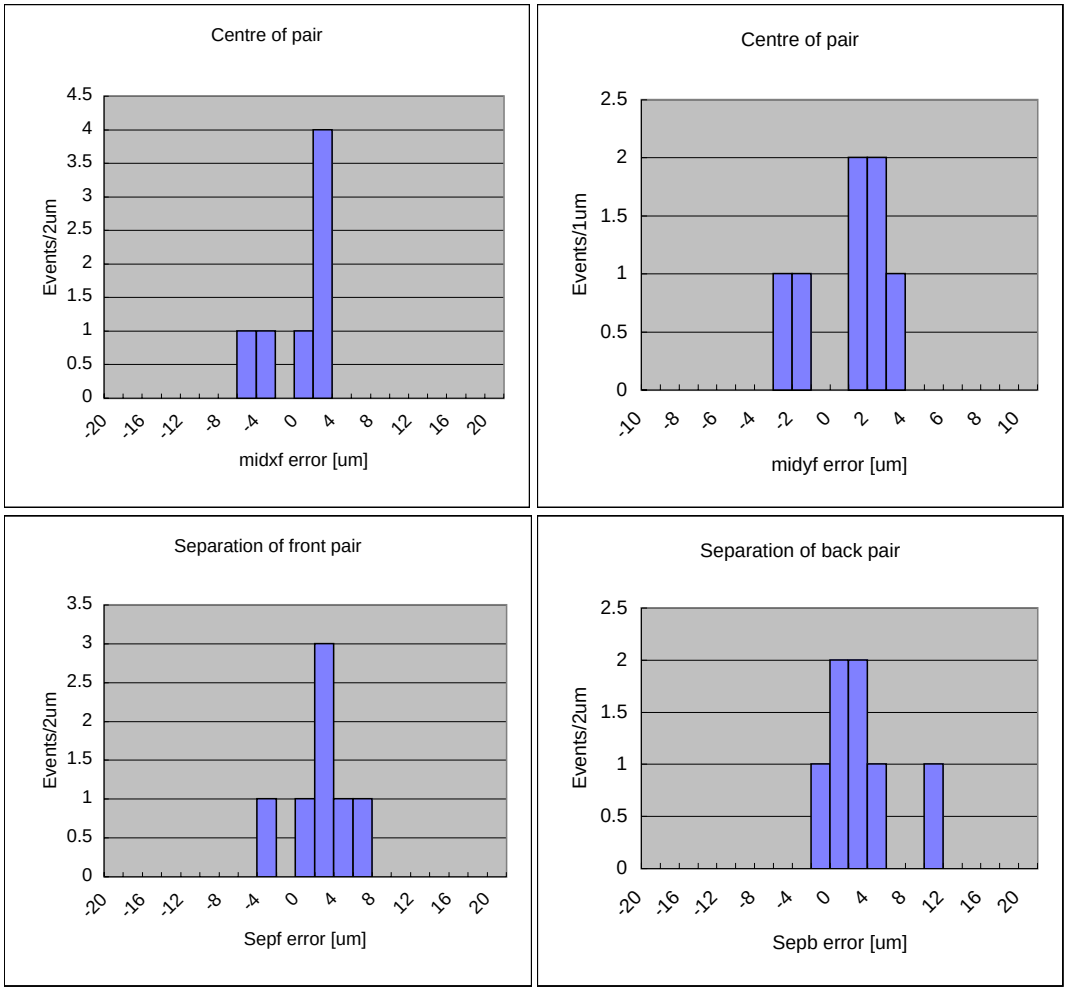

Figure 3 In-plane survey: deviations from the nominal of the centre of the front pair of sensors, midxf and midyf, and the separation of the front pair, sepf, and the back pair, sepb

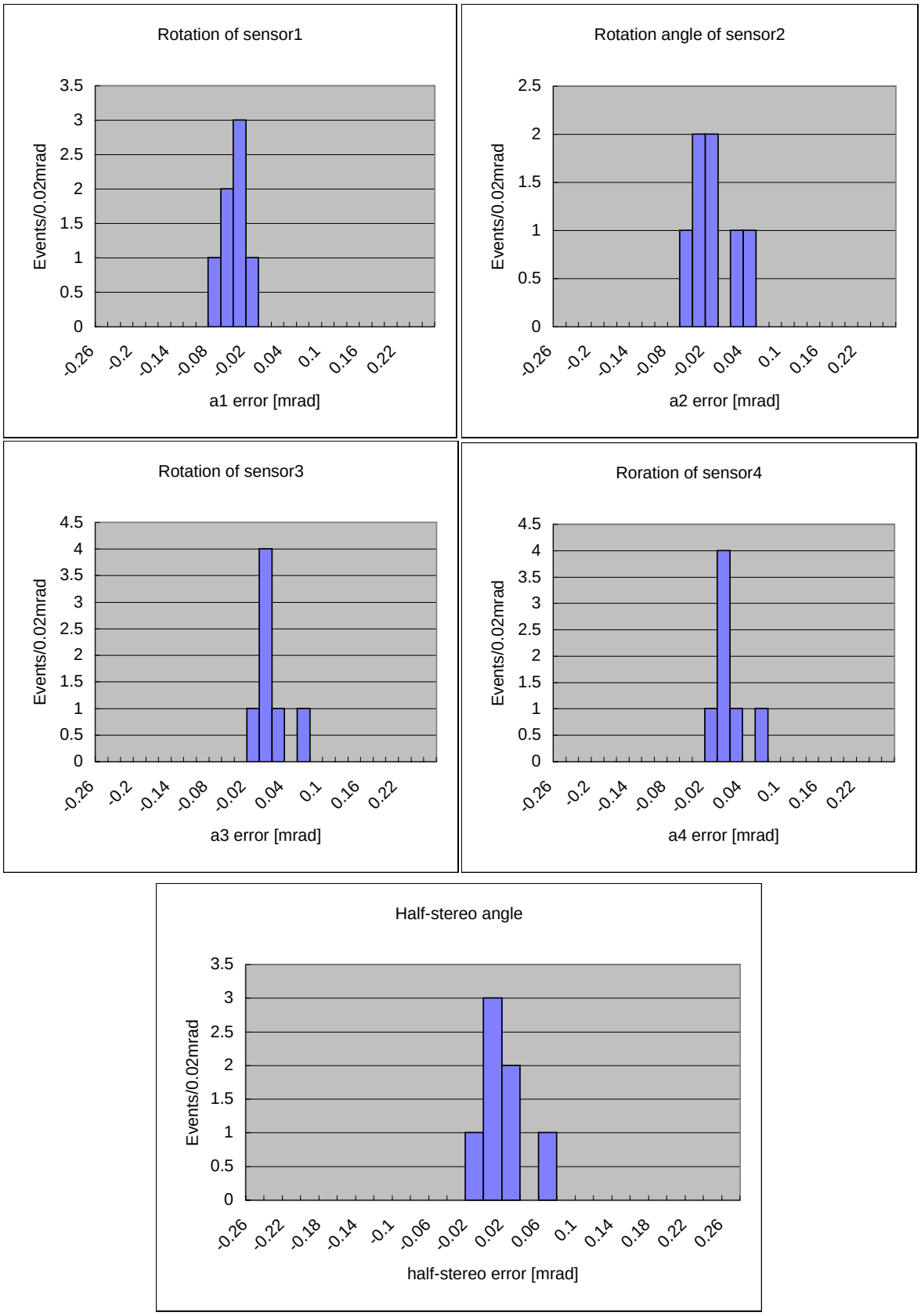

Figure 4 In-plane survey: deviations from the nominal of the rotations of the sensors, a1, a2, a3, and a4, and the half-stereo angle

2.3 Out-of-Plane Survey

Two tolerance limits are placed on the out-of-plane deviations, as described in SCT-BM-FDR-7. One is the maximum deviation of the z-height of the sensor surface from the nominal, which should be <200 μm. The other is that the maximum z-flatness residual, after the 'minimal use' of the z data, should be < 50 μm.

2.3.1 Maximum z Deviations

Results are presented on the z-profiles of 8 modules constructed by the Japanese cluster and measured at KEK using a 3D metrology machine. The z coordinates at three locations Z1, Z2 and Z3 on the BeO facings, as defined in Figure 1 of SCT-BM-FDR-7, are used to define a plane. The nominal half-thickness of the BeO facing – VHCPG baseboard assembly, 0.46 mm, is added to this measured plane, to define the *module plane*. The nominal top and bottom sensor surfaces are at +0.575mm and -0.575 mm from the module plane, respectively, since the nominal module thickness is 1.15mm in the sensor area. The deviations of the z-heights of the top and bottom sensor surfaces from the nominal are measured. The distribution of the maximum z deviation from the nominal for both sides of each module is shown in the left-hand plot of Figure 5.

It is seen that all the modules satisfy the tolerance of 200 μm for the maximum deviation of the z-height of the sensor surface from the nominal. The majority of data are within ±80 μm. Two module surfaces are outside this range; one module giving +83 μm for its top surface and a different module giving -176 μm for its bottom surface.

2.3.2 Minimal z Errors

In order to systematise the deviations in z seen above, the 'minimal use' of z data has been applied, as described in Appendix 1 of SCT-BM-FDR-7. After fitting the mid-planes of the modules, separately for the left and right sides, the 'minimal z' profiles from the fitted mid-plane are measured. These are averaged over the sample of 8 modules to obtain the *mean profile*. The 'minimal z'-profiles are shown for a typical module in Figure 6, together with its 'minimal z errors', that is, the deviations from the mean profile.

The top-left plot of Figure 6 shows the z-coordinates of the surface of the four sensors along the strip direction for different lateral positions. The bottom-left plot shows the z-coordinates, perpendicular to the strips, for different longitudinal positions. It is seen that the top and bottom sensors are symmetric and curling inwards towards the ends of the module where the sensors are free from the baseboard. This is caused by the intrinsic bow of the sensors.

The minimal z errors are shown in the right-hand plots of Figure 6. The top-right plot shows the z deviation from the mean profile along the strip direction for different lateral positions, for all four sensors. The bottom right plot shows the z deviation from the mean profile perpendicular to the strip direction for different longitudinal positions, for all four sensors.

The distribution for all modules of the maximum of the 'minimal z errors' of four sensors is shown in Figure 5, in the top-right plot, and the rms of the 'minimal z error' is shown in the bottom-right plot. It is seen that the maximum deviation of any sensor from the mean profile is below 30 μm, and the rms of this deviation is less than 10 μm. Thus all these modules satisfy the specification of a deviation of <50 μm from the mean profile.

The out-of-plane specifications can therefore be met with the present assembly jigs, assembly processes and module components.

Figure 5: Out-of-plane survey: the left-hand plot shows the maximum measured z deviations of sensors from the nominal top and bottom module surfaces. The right-hand plots show the results after the 'minimum use' of z data; top right the resulting maximum z errors of the 4 sensors, and bottom right the rms of the z errors of the 4 sensors.

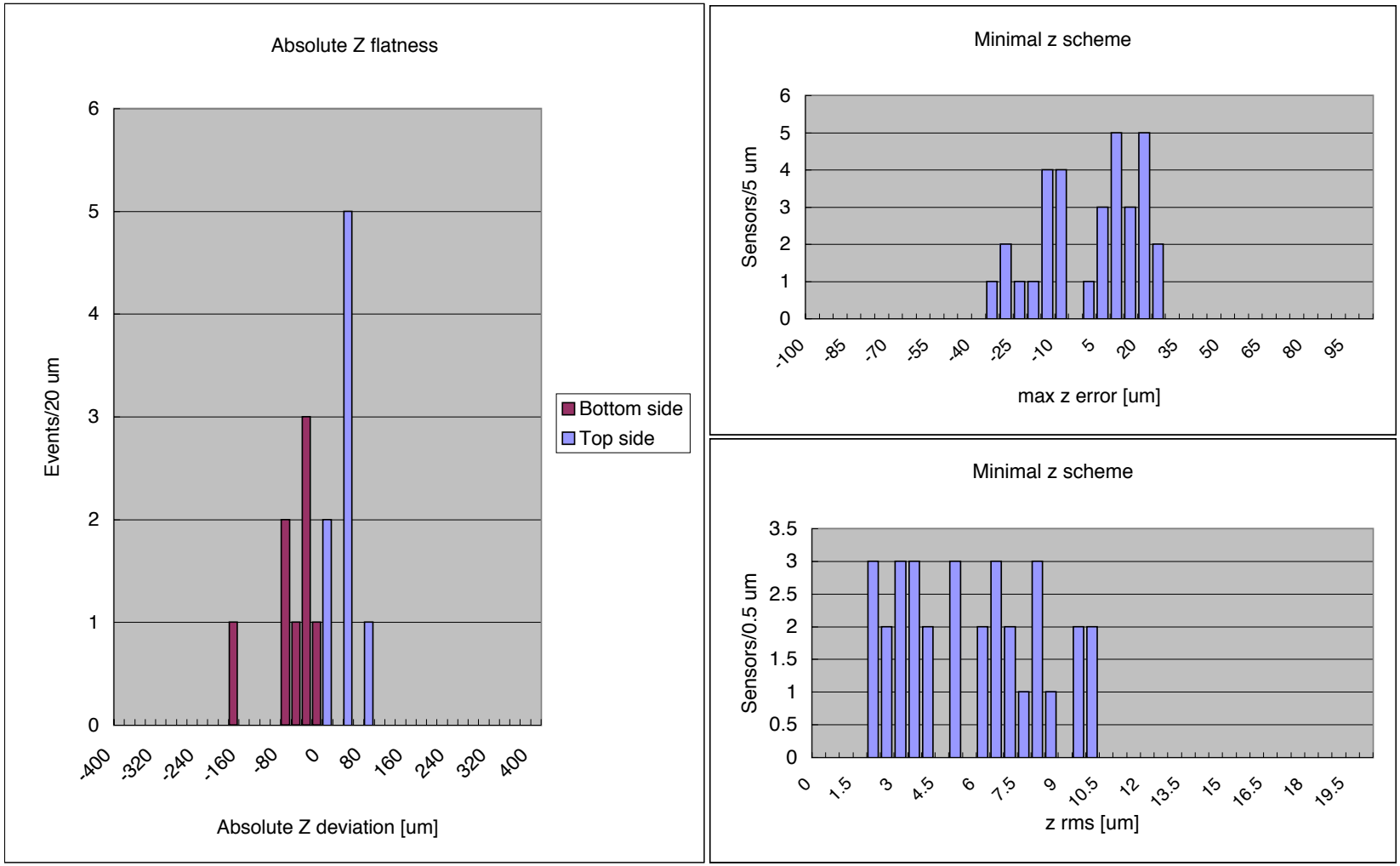

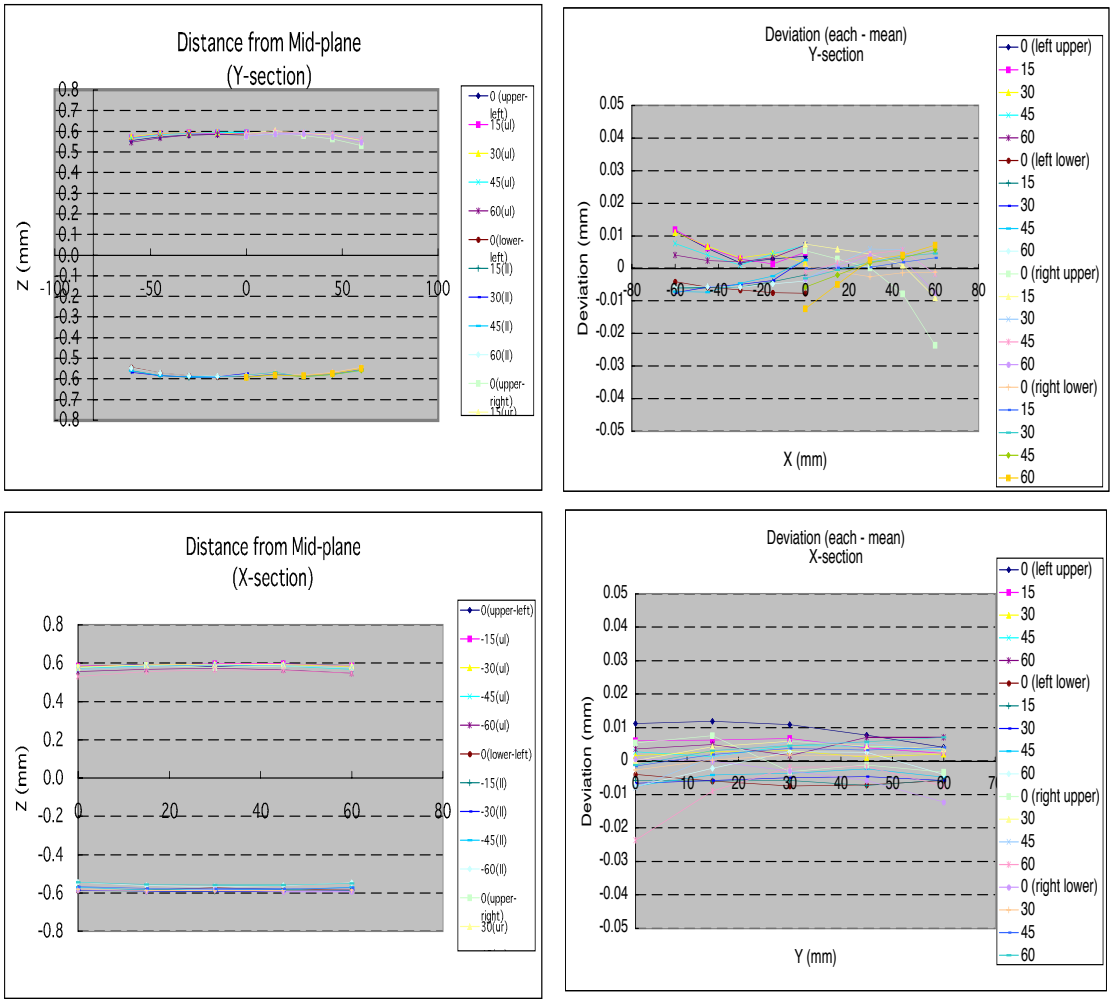

Figure 6: Out-of-plane measurements for module 20220170100035. The top-left plot shows the z-coordinates of the surface of the four sensors along the strip direction for different lateral positions. The bottom-left plot shows the z-coordinates, perpendicular to the strips, for different longitudinal positions. The top-right plot shows the z deviation from the mean profile along the strip direction for different lateral positions, for all four sensors. The bottom right plot shows the z deviation from the mean profile perpendicular to the strip direction for different longitudinal positions, for all four sensors.

2.3.3 Thermal Cycling and Long-term Tests

A number of modules have been subjected to thermal cycling and long-term readout tests. The thermal cycle sequence was from room temperature to –30 ^{o}C and +60 ^{o}C, repeated 5 times. In the long-term tests, the module was operated, with hybrid power on, for 24 hrs with the hybrid temperature at around 30 ^{o}C. The same in-plane and out-of-plane metrology was repeated after the thermal cycles and the long-term test.

The in-plane surveys show that there is essentially no change in the in-plane parameters. The changes in the out-of-plane measurements before and after thermal cycling and long-term testing are shown in Figure 7. The left plot shows the change in the maximum z deviations before and after the thermal cycles, and the right plot before and after the long-term tests.

Figure 7: Out-of-plane survey: change in the maximum z deviation before and after thermal cycling (-30 ^{o}C to +60 ^{o}C, 5 times) (left). And change following the thermal cycling after the long-term test (24 hours operation, hybrid power on) (right).

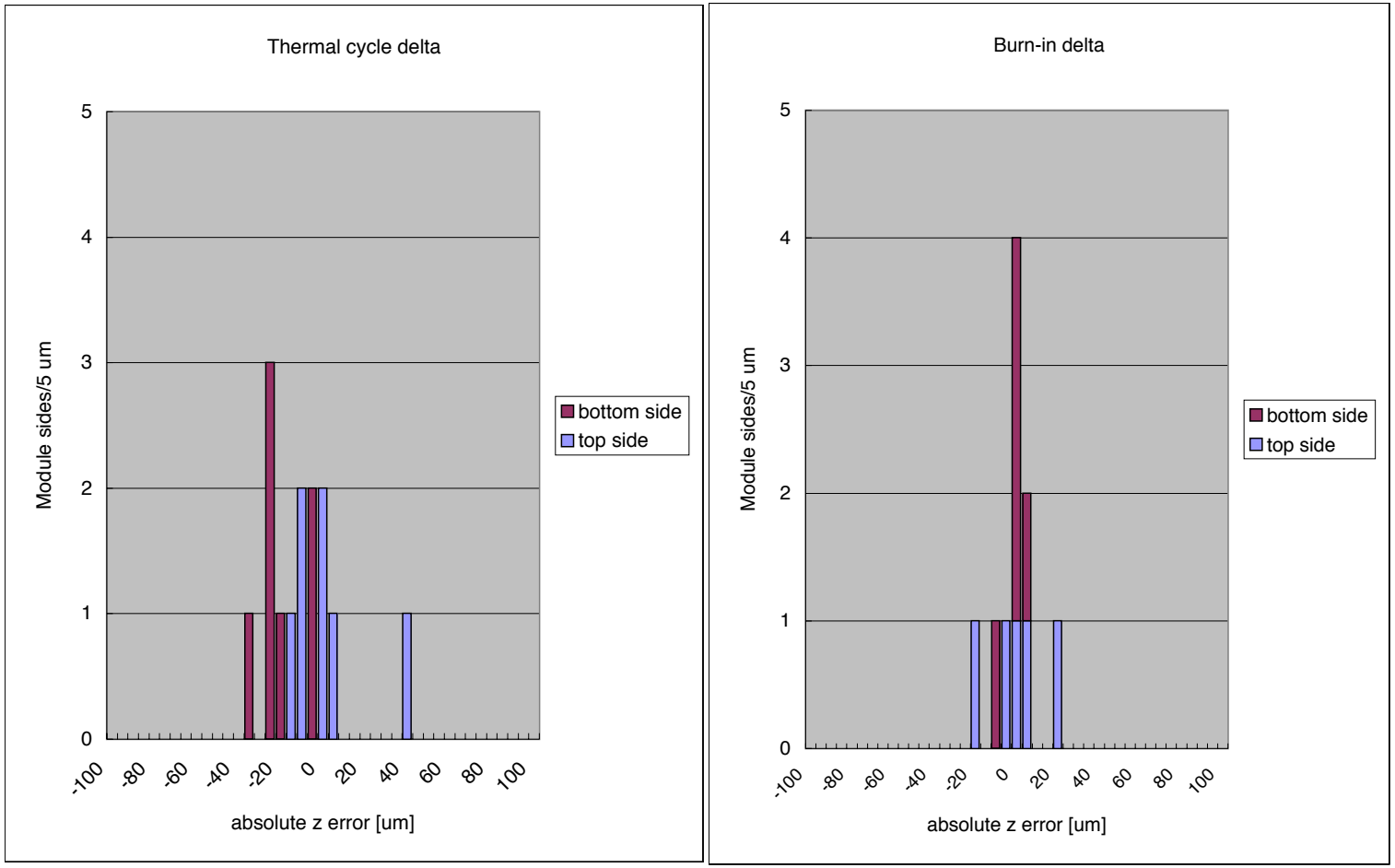

Since the long-term test is a steady-state operation, no change is anticipated. The distribution shows that the majority of the data are within 10 μm, with a few points extending out to 20 μm. These data are comparable with the measurement errors of the metrology machine, although the larger values could be caused by a real deformation.

Thermal cycling is more dynamic and some deformation is anticipated. As seen from the plot, the majority of results are within 20 μm, and comparing these data with the long-term test distribution, there could be a deformation of order 10 μm or less. One module, however, showed a larger deviation of 41 μm. This was the module that showed the second largest deviation before thermal cycling. The maximum z deviation of this module was changed from 83 μm before to 123 μm after the thermal cycles.

Although there is some deformation associated with thermal cycling, all modules still have a maximum z deviation of <200 μm. Also, all modules satisfy the tolerance of <50 μm for the minimal z errors.

3 BARREL MODULE THERMAL RESULTS

3.1 Thermo Profile Measurements made with a Thermo Viewer

The temperature profile has been measured for a sample of unirradiated modules by using a thermo viewer. Although a thermo viewer measurement is desirable because of its remote sensing nature, it involves the following practical difficulties:

(1) estimating or determining the reflectivity of the surface, which depends on the surface and the material

(2) shielding infra-red light from the external environment

(3) the infra-red transparency of silicon

The transparency of silicon to infra-red wave-lengths precludes the measurement of the temperature of the silicon sensors. Thus the measurement is only useful for estimating the temperature of the hybrids and the BeO facings. Thermo viewing is not a technique that will be used for every module during production, but can be a useful diagnostic tool.

A typical example of the measured temperature profile of the hybrid and of the facing is shown in Figure 8, with an ASIC power of 5.3 W. In the figure, the temperatures are given with respect to the top of the BeO cooling facing. With respect to this, the highest temperature on the hybrid was 11 – 12 ^{o}C at the location of the ASICs. The temperature at the hybrid thermistor was about 6^{o}C. The thermal FEA simulation is consistent with these measurements. This is illustrated in Figure 9, which shows a thermal simulation of the hybrid plus ASICs with the same ASIC power of 5.3W. The highest temperature of the hybrid with respect to the BeO cooling facing is about 12^{o}C, as in the data.

Figure 8 The thermo profile of the hybrid of a module measured with a thermo viewer. The temperatures are normalised to the temperature of the top of the BeO cooling facing.

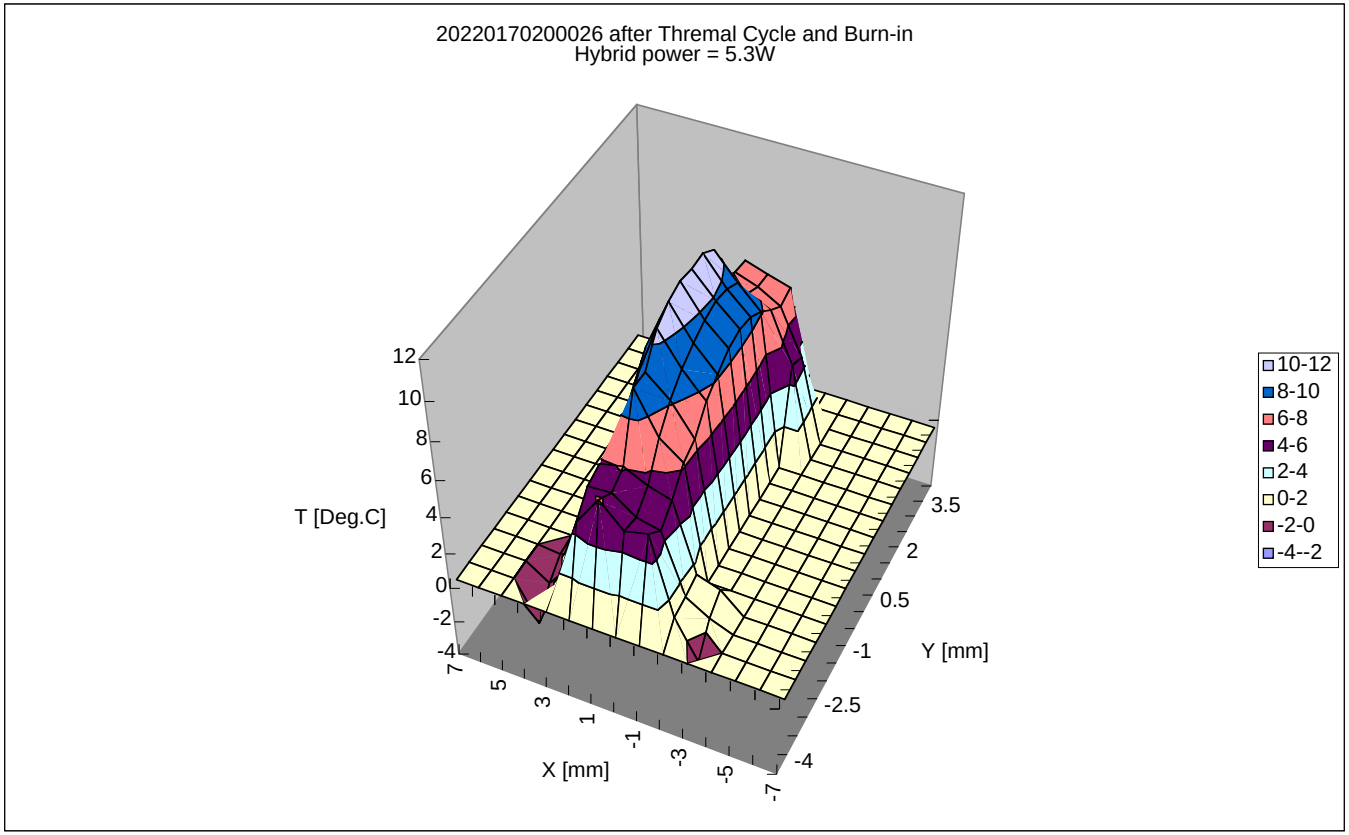

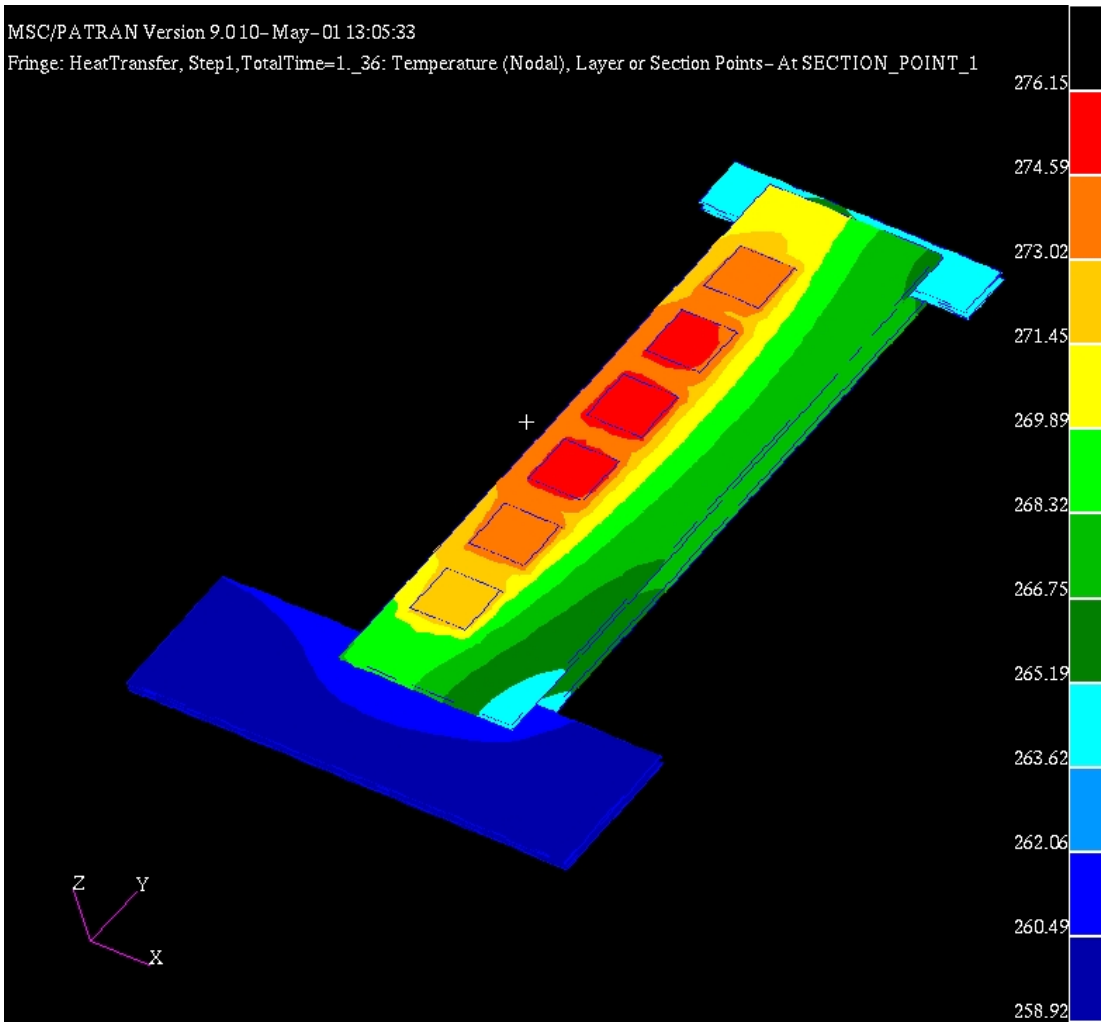

Figure 9: FEA simulation of a hybrid and ASICs, with an ASIC power of 5.3W.

3.2 Thermal Module Results

3.2.1 Thermally Induced Distortions.

Studies have been carried out on the elastic and non-elastic thermally induced distortions on barrel SCT mechanical modules. A total of four modules were built, using non-electrically working but thermally realistic components. Each module was measured under a non-contact 3D metrology system with a measurement accuracy of better than 1μm in the 'xy' plane and around 4μm in the 'z' plane. The 'z' measurements are made by an automated depth of focus algorithm running at high (x800) magnification. Each module was then heated and cooled over a temperature range of +39˚C to –17˚C. At five specific temperatures (-17˚C, -6˚C, +7˚C, +21˚C and +39˚C) the module was allowed to reach equilibrium and the profile measurements were repeated.

Each module was then thermally cycled ten times between -30˚C and +100˚C in a nitrogen atmosphere and the profile re-measured. No variations in the 'xy' measurements were observed. The 'z' variations were only measurable at the unsupported corners of the detectors. The average

movement seen over all temperature variations for the 4 modules, prior to thermal cycling, was 1.29µm/˚C. After thermal cycling, the average value was found to be 1.33µm/˚C, that is, essentially unchanged.

An allowance for elastic deformation will be applied to room temperature survey data to predict the final module shape at the operating temperature.

3.2.2 Thermal performance.

A module has been built using irradiated p-in-n silicon detectors. The detectors were assembled to a pre-series BeO/VHCPG baseboard and the thermal module was completed by the addition of a pre-series copper/kapton hybrid, complete with carbon-carbon bridge supports. The detectors were biased in the normal way and the front-end chips were simulated using 2.2Ω silicon chip heaters. The module was equipped with a number of Pt100 thermal sensors, as illustrated in Figure 10, that provided temperature readout of the two hybrid bridges, three of the detector corners, the upper cooled facing, the cooling block and the ambient gas temperature. The cooling was provided by a mixture of water and antifreeze flowing in a copper pipe, and the cooling interface was a copper block of approximately correct dimensions brazed to the pipe. The block was connected via thermal grease (DC 340) to a 3 mm thick piece of aluminium frame and this in turn was connected to the beryllia facing of the module through another layer of DC 340. The pipe and cooling block were sprung so that the connection of the aluminium to copper was by spring pressure. The connection of the facing to the aluminium was by screws. The layout is thus representative of the principles to be used in the final SCT.

A summary of the results to-date are given in Tables 2 and 3.

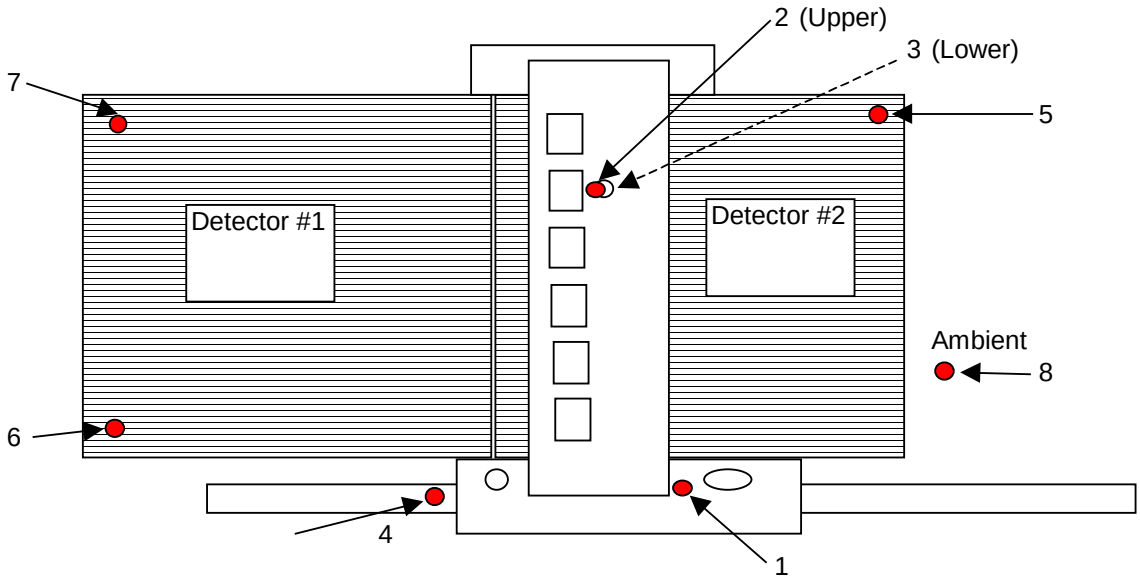

Figure 10: Layout of the thermal module, showing the positions of the temperature sensors, labelled 1 to 8.

Hybrid power (W)	Detector power (W)	Coolant ^{o}C	Ambient ^{o}C .	Cooled facing ^{o}C	Hottest hybrid ^{o}C	Hottest detector ^{o}C
0	0	-6.82	-6.03	-4.03	-3.90	-4.31
6.36	0	-7.52	-5.16	0.96	12.53	1.95
6.35	0.52	-7.51	-4.64	1.70	13.56	3.09
6.35	1.01	-8.02	-4.47	2.04	14.04	3.36
6.35	0.28	-6.84	-4.19	1.85	13.63	3.14
8.11	0.00	-8.52	-4.19	2.73	17.52	4.11
8.11	0.35	-7.33	-4.01	3.13	18.11	4.76
8.11	0.65	-7.54	-3.70	3.49	18.67	5.43
8.11	1.30	-6.95	-3.52	4.08	19.58	6.37
8.11	1.24	-10.13	-7.48	-0.42	15.14	2.32
8.12	1.64	-10.93	-8.73	-1.45	14.08	1.40
8.12	3.03	-11.25	-6.43	-0.24	15.61	3.18
8.30	3.32	-10.34	-4.99	1.65	18.09	5.51

Table 2: Thermal module temperatures as a function of hybrid and detector power

Hybrid power	Detector power	δT coolant – facing	δT facing - hybrid	δT facing - detector	δT ambient - coolant
0.00	0.00	2.79	0.13	-0.28	0.79
6.36	0.00	8.48	11.58	0.99	2.36
6.35	0.52	9.20	11.86	1.40	2.87
6.35	1.01	10.06	12.00	1.33	3.55
6.35	0.28	8.69	11.77	1.29	2.65
8.11	0.00	11.25	14.79	1.39	4.33
8.11	0.35	10.46	14.98	1.63	3.32
8.11	0.65	11.03	15.18	1.94	3.83
8.11	1.30	11.03	15.50	2.29	3.44
8.11	1.24	9.71	15.56	2.74	2.65
8.12	1.64	9.48	15.53	2.86	2.20
8.12	3.03	11.00	15.86	3.42	4.81
8.30	3.32	11.98	16.44	3.86	5.35

Table 3: Differential temperatures as measured on a thermal module

The module has been designed using FEA that has been verified up to thermal runaway through previous thermal module prototypes. The present experimental results show stable running at a coolant temperature of around –10.5 ^{0}C with a detector power dissipation of about 130 μW/mm^2 normalised to 0 ^{o}C. The FEA predicts thermal runaway at around 135 μW/mm^2 at such a coolant temperature. Thus the results confirm the designed thermal operation of the module, that is, its

stable operation and large safety factor against thermal runaway with the envisaged coolant temperatures of ATLAS.

4. SUMMARY

The metrology data show that the module design, components and assembly methods are appropriate to the SCT specifications. Thermal data support the FEA calculations used to optimise the module design, and hence the thermally robust nature of the barrel module.